Carbon 148 (2019) 72–79

Contents lists available at ScienceDirect

Carbon

journal homepage: www.elsevier.com/locate/carbon

Enhanced nonlinear absorption and ultrafast carrier dynamics in graphene/gold nanoparticles nanocomposites

Yang Yu, Jinhai Si*, Lihe Yan, Ming Li, Xun Hou

Key Laboratory for Physical Electronics and Devices of the Ministry of Education & Shaanxi Key Lab of Information Photonic Technique, School of Electronics & Information Engineering, Xi'an Jiaotong University, Xi'an, 710049, China

ARTICLE INFO

Article history:
Received 28 December 2018
Received in revised form
2 March 2019
Accepted 21 March 2019
Available online 23 March 2019

ABSTRACT

The nonlinear optical response of gold nanoparticles/reduced graphene oxide (AuNPs/rGO) nanocomposites prepared by laser ablation method was studied using a femtosecond laser open-aperture (OA) Z-scan method, and an enhanced nonlinear absorption effect was observed. Using the femtosecond time-resolved pump-probe measurements, the nonlinear response mechanism in the hybrid was studied. When graphene was excited by an ultrashort laser pulse, the bleaching of valence band (VB) and the filling of conduction band (CB) took place, causing a saturable absorption (SA) effect. When decorated with gold nanoparticles, the excited carriers from the CB of graphene could transfer to the sp band of the metal before returning to the VB of graphene. This process would take place in a much longer time scale (~50 ps) than the direct relaxation in pure graphene, causing the enhancement of the SA effect. The excited carrier dynamics were further demonstrated using femtosecond time-resolved transient absorption spectroscopy, and the interband relaxation of the excited electrons from the sp band of AuNPs to the CB of graphene was observed, resulting in the further filling of the CB of graphene and enhancement of the SA effect.

1. Introduction

As a two-dimensional carbon nanomaterial, graphene has attracted remarkable research interests in recent years due to its unique electronic, optical, and mechanical properties [1–3]. As pure graphene has a zero bandgap and the Fermi level is at the intersection of V-shaped conduction band (CB) and the valence band (VB) at the K point of the Brillouin zone, light at any wavelength can be possibly absorbed in optical applications [4,5]. Because of this special optical property, when graphene is irradiated by an ultrashort laser pulse, the top of the VB will be bleached and the bottom of the CB will be filled. If the pulse width of irradiated laser is shorter than the relaxation lifetime of the carriers, no more electrons can be further excited resulting in the reduction of the further absorption, namely, saturable absorption (SA) effect. Due to its excellent SA property, graphene has been successfully used as saturable absorber in some mode-locked laser working in the visible to mid-infrared region [5,6].

Recently, noble metal/graphene oxide (GO) nanocomposites have attracted much attention due to their enhanced linear and nonlinear optical (NLO) properties. The abundant oxygen-containing groups in graphene oxide (GO) make it possible for chemical functionalization of the material [7,8]. For example, strongly enhanced nonlinear absorption and refraction are observed in graphene oxide (GO) film with gold nanoparticles (AuNPs), and the enhanced nonlinearity is attributed to the efficient energy and/or charge (electron) transfer upon photoexcitation and the synergistic coupling effects between AuNPs and GO [9]. The optical nonlinearity of silver-decorated graphene has been systematically studied using a Z-scan technique, and the strong SA in the composite was attributed to the electronic interaction between graphene and silver NPs [10]. Generally, charge transfer between graphene and metal NPs is considered to be the main factor in achieving the enhancement of nonlinearity of the composite. Although some theoretical models have already been proposed to explain the mechanism of the enhancement of NLO properties and the carriers relaxation process between metal NPs and graphene [9,10], the direct experimental evidence is still lacking.

Femtosecond time-resolved pump-probe and transient absorption (TA) measurements can provide effective tools to investigate the carrier dynamics of the various materials. Ultrafast optical

* Corresponding author.
E-mail address: jinhaisi@mail.xjtu.edu.cn (J. Si).

https://doi.org/10.1016/j.carbon.2019.03.054
0008-6223/

pump-probe spectroscopy has been used to measure carrier relaxation times in graphene, and two distinct relaxation processes of nonequilibrium photogenerated carriers were observed: intraband electron-electron scattering (~100 fs) and slow electron-phonon scattering (>1 ps) [11,12]. Some efforts have also been devoted to study the photoinduced electron transition and relaxation dynamics in nanostructured metals using femtosecond TA spectroscopy [13]. Nevertheless, the photoinduced carriers kinetics in graphene/metal NPs composites, especially the transition processes of electrons between graphene and nanostructured metals, are still ambiguous and further experimental proof are needed.

In this work, we prepared rGO/AuNPs nanocomposites using laser ablation method. The NLO properties of GO, rGO and AuNPs/rGO are studied by open aperture (OA) Z-scan technique using a Ti: sapphire femtosecond laser. The results show that AuNPs/rGO hybrid exhibit enhanced NLO properties compared with GO and rGO. By adjusting the laser power, irradiation time and Au^{3+} ion concentration, the optical and nonlinear optical of the products are well controlled. Femtosecond time-resolved pump-probe technique is used to investigate the nonlinear response dynamics of the material, the relaxation time of which was estimated to be 1 ps, indicating the excited carriers transfer from the CB of graphene to the sp band of AuNPs. This process was further demonstrated using femtosecond time-resolved transient absorption (fs-TA) spectroscopy, and the interband relaxation of the excited electrons from the sp band of AuNPs to the CB of graphene was observed, resulting in the further filling of the CB of graphene and enhancement of the SA effect.

2. Materials and methods

The rGO/AuNPs nanocomposites are prepared using femtosecond laser ablation method [14–18]. 2 mg of GO was dispersed in 10 mL of distilled water using ultrasonic treatment for a few hours until a homogeneous yellow solution was obtained. To synthesis the AuNPs/rGO nanocomposites, an appropriate amount of $HAuCl_4$ solution (0.025 mmol mL^{-1}) was added into the GO solution. Then, the 10 mL of solution was put into a beaker for laser processing. Femtosecond laser pulses, generated by a mode-locked Ti: sapphire laser (central wavelength: 800 nm, pulse width: 100 fs, repetition rate: 1 kHz), was focused into the solution by a lens with a focal length of 100 mm. To make the solution to be irradiated homogenously, a magnetic stirrer was used during the laser irradiation process.

Transmission electron microscopy (TEM) and high resolution TEM (HRTEM) images were performed using a JEM-2100 Plus microscope to study the morphology of the nanocomposites. Raman spectra were performed using a Laser Raman Spectrometer with excitation wavelength at 633 nm. X-ray photoelectron spectroscopy (XPS) were performed using an ESCALAB Xi + XPS spectrometer. UV–Vis absorption spectra were performed using a UV-2600 spectrophotometer in a quartz cuvette.

The NLO properties of the as-prepared products were studied using an OA Z-scan system. The femtosecond laser was as the same as mentioned above. The laser pulses are focused into the sample by a 20 cm lens. All samples were obtained by dropping different nanomaterial solutions on glass slides and dried at 40 °C. The thickness of the GO and its hybrids films are estimated to be about 100 nm.

Femtoseocnd time-resoved pump-probe and TA measuremetns were used to study the photoinduced carriers dynamics in the composits. In the femtoseocnd time-resoved pump-probe experiments, pump pulses centered at 800 nm with energies of 1 μJ were used to generate photoexcited carriers, while weak probe pulses with the same wavelenth are used to measure the changes in the transmittivity of the samples at various delays. The pump and the probe were focused to a spot size of about 200 μm, and the pump pulse energy intensity was estemited to be about 3.2 mJ cm^{-2}.

In the TA measurements, the output of the laser was split into two parts: the stronger beam was used as the excitation light, and the other beam was focused into a 1-mm-thick sapphire plate to generate the broadband white-light probe pulses from 450 nm to 750 nm. The transmitted probe pulses from the sample were collected by a fibre-coupled spectrometer connected to a computer. The TA data were recorded as a function of the delay time between the pump and probe pulses.

3. Results and discussions

Firstly, AuNPs/rGO composites were synthesized using femtosecond laser ablation in liquids (LAL) method. LAL method could provide a green one-step synthesis strategy of nanomaterials, such as carbon nanodots (C-dots) and graphene oxide composites [14–18]. During the laser irradiation process, when femtosecond laser irradiates into GO aqueous solution containing appropriate metal ions, plasma plume and bubbles can be created due to the high temperature, high pressure induced by the laser pulses. As a consequence, highly reactive species are produced and reactions between these species result in NPs formation, as well as the reduction and doping of GO. We systematically studied the effect of laser power, irradiation time, and Au^{3+} ion concentration on the optical property and morphology of the products. Fig. 1(a) shows the absorption spectra of GO, rGO, and AuNPs/rGO prepared with different irradiation time. The laser power was fixed at 300 mW, and the Au^{3+} ion concentration is 1.5 mM. From the figure we can see that, a characteristic shoulder at 305 nm which is attributed to the $n \rightarrow \pi^*$ transitions of C=O bonds can be observed in GO [19]. As a comparison, the disappearance of absorption shoulder at 305 nm and the increase of absorption in the whole visible light ranges of rGO indicate the reduction of GO and the formation of rGO after laser irradiation (The color change of GO before and after laser irradiation are given by inset (i) and (ii) of Fig. 1(b)). When GO solution mixed with Au^{3+} ions is reduced, the color of the solutions change to claret (as shown by inset (iii) of Fig. 1(b)), and an obvious absorption peak near 525 nm is observed due to the surface plasmon resonance (SPR) of AuNPs [20,21]. With increasing the irradiation time from 10 min to 1 h, the SPR peak of AuNPs is enhanced indicating that the reduction degree of the Au^{3+} ions is increased. In addition, the absorption peak of AuNPs shows a slight blue shift with increasing the irradiation time, which might be due to the influence of rGO [22]. With prolonging the irradiation time, the reduction degree of GO increases gradually, which leads to the enhancement of absorption in the blue-light region and the blue shift of absorption peak of the composites [17,22–24]. The obvious absorption peak near 310 nm is attributed to the electron transfer from Cl atom to Au atom of $HAuCl_4$ [21]. Because of the exhausting of the Au^{3+} ions, the peak near 310 nm disappears and the increment of the SPR peak intensity saturates when the irradiation time is increased to be more than 1 h. Besides, the influences of laser power and concentration of Au^{3+} ions were also investigated, and the absorption spectra results are given in Fig. S1 and S2, respectively.

To study the morphology change of the AuNPs decorated on the rGO nanosheet at different experimental conditions, TEM imaging was explored. Fig. 2(a)-(f) show the TEM images of AuNPs/rGO composites prepared with different irradiation time. The laser power was adjusted to 300 mW and the Au^{3+} ions concentration was fixed at 1.5 mM. The insets in the upper left corner of Fig. 2(a)-(f) show the corresponding high-resolution TEM (HRTEM) image of AuNPs. Obvious lattice fringes with the spacing of 0.24 nm and

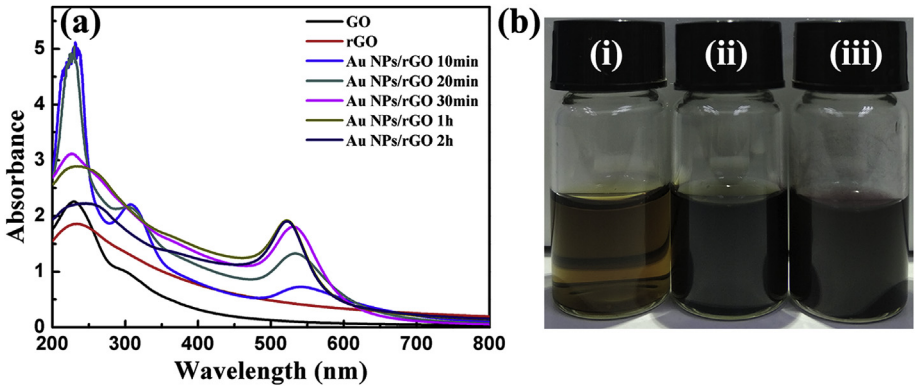

Fig. 1. Absorption spectra of the products prepared **(a)** with different irradiation time (Au ions concentration fixed at 1.5 mM, and laser power fixed at 300 mW). **(b)** Photographs of **(i)** GO, **(ii)** rGO, and **(iii)** AuNPs/rGO composites prepared irradiated by 300 mW laser for 30 min with Au^{3+} ions concentration of 1.5 mM. (A colour version of this figure can be viewed online.)

0.20 nm are observed, which can be attributed to the (111) and (200) plane of the Au crystallite, respectively [25,26]. The insets in the upper right corner of Fig. 2(a)-(f) show the corresponding size distributions of the AuNPs. After 10 min of irradiation (Fig. 2(a)), AuNPs are obviously produced. The size of the particles is mainly concentrated in 0.5–3 nm. With increasing the irradiation time to 20 min (Fig. 2(b)), large particles centered at 4.35 nm begin to appear. The formation of the large NPs could be mainly due to two reasons: firstly, the continuous growth of the small AuNPs after subsequent laser irradiation; secondly, the formed small AuNPs might be re-melted and aggregated together forming large NPs with lower concentration. Fig. 2(c) and (d) show the morphologies of the sample prepared after 30 min irradiation. Small particles centered at 2.03 nm (Fig. 2(c)) and large particles centered at 17.6 nm (Fig. 2(d)) are observed at different areas of the sample. When the irradiation time is increased to 1 h (Fig. 2(e)) and 2 h (Fig. 2(f)), almost only large particles can be observed and the particle size has no significant difference anymore. Generally, AuNPs with high concentration can be quickly formed after a short-time irradiation; with prolonging the irradiation time, the growth and melting/aggregation will form AuNPs with larger size and lower concentration.

XPS and Raman spectra were used to study the chemical structure of the AuNPs/rGO composites. Fig. 3(a) shows the evolution of the C 1s XPS spectra of the composites prepared with different irradiation time. Peaks at 284.5, 286.6, and 288.5 eV which are attributed to C=C, C–O, and C=O groups are observed in both samples [27,28]. It's evident that, the gradual decease of C–O group with prolonging the irradiation time indicating that the reduction degree of GO is enhanced. As a comparison, the C 1s XPS spectra of GO and rGO is shown in Fig. S3 and S4, respectively. The Au 4f XPS spectra of AuNPs/rGO is shown in Fig. S5. The two peaks centered at 84 and 87.7 eV are corresponding to the binding energies of Au $4f_{7/2}$ and Au $4f_{5/2}$ of Au, respectively [29].

Fig. 3(b) gives the Raman spectra of GO, rGO, and AuNPs/rGO samples. Two characteristic peaks near 1330 cm^{-1} corresponding to the D band which is attributed to disorder or defects in carbon atoms band, and 1590 cm^{-1} corresponding to the G band which is attributed to the sp^2 in-plane vibration of carbon atoms, can be observed [30]. Besides, compared to GO and rGO, significant enhancement of Raman spectrum of AuNPs/rGO can be observed due to the surface enhancement effect of the AuNPs [30,31]. Furthermore, the surface enhancement effect of the AuNPs is strengthened with more AuNPs are produced by prolonging the irradiation time. Because of a lower AuNPs concentration at longer irradiation time, when the irradiation time increases to 2 h, there has a drop in the Raman intensity, which may be due to decrease of the concentration of AuNPs in the area of the exciting laser spot.

To study the nonlinear property of the as prepared AuNPs/rGO hybrids, an open-aperture Z-scan technique was used. To control the doping concentration of the AuNPs, the irradiation time varied from 10 min to 2 h, while the laser power and concentration of Au^{3+} was fixed at 300 mW and 1.5 mM, respectively. In the experiments, femtosecond laser centered at 800 nm was focused with a lens of 200 mm focal length with a pulse energy of 50 nJ. All samples were obtained by dropping different nanomaterial solutions on glass slides and dried at 40 °C. Fig. 4(a) show the normalized nonlinear transmittances as functions of the z-position in GO, rGO, and AuNPs/rGO. Both the rGO and AuNPs/rGO are ablated by femtosecond laser for 30 min. It is clearly seen that, with increasing the incident light intensity, the transmittances in all samples increased. As no nonlinear scattering signal was observed in the experiments, the increase of the transmittance could be attributed to nonlinear absorption (NLA) effect in the sample. Compared with GO, the SA property of rGO is enhanced, while those for AuNPs/rGO is further improved. Fig. 4(b) shows the normalized nonlinear transmittances as functions of the Z-position in AuNPs/rGO with different irradiation time. When the irradiation time is less than 1 h, the SA property is increased with increasing the irradiation time. While for 2 h, a significant reverse saturable absorption (RSA) signal can be also observed besides SA behavior.

Usually, the dominant mechanisms of the NLO effects are attributed to the third-order nonlinear optical effects in Z-scan experiments, and the nonlinear absorption coefficient $\alpha(I)$ can be expressed as [10,32,33].

$$\alpha(I) = \frac{\alpha_0}{1 + I/I_s} + \beta I \tag{1}$$

where α_0 is the linear absorption coefficient, I_s is the saturation intensity, and β is the RSA coefficient. The differential equation that the beam propagation in an absorber is

$$\frac{dI}{dl} = -\alpha(I)I \tag{2}$$

where l is the propagation thickness in absorber. Using equations (1) and (2), the simplified calculation result of transmittance T is

$$T(z) = \exp\left(- \left(\frac{\alpha_0}{1 + I(z)/I_s} + \beta I(z) \right) l_0 \right) \tag{3}$$

where l_0 is the thickness of the film. The waist radius of Gaussian

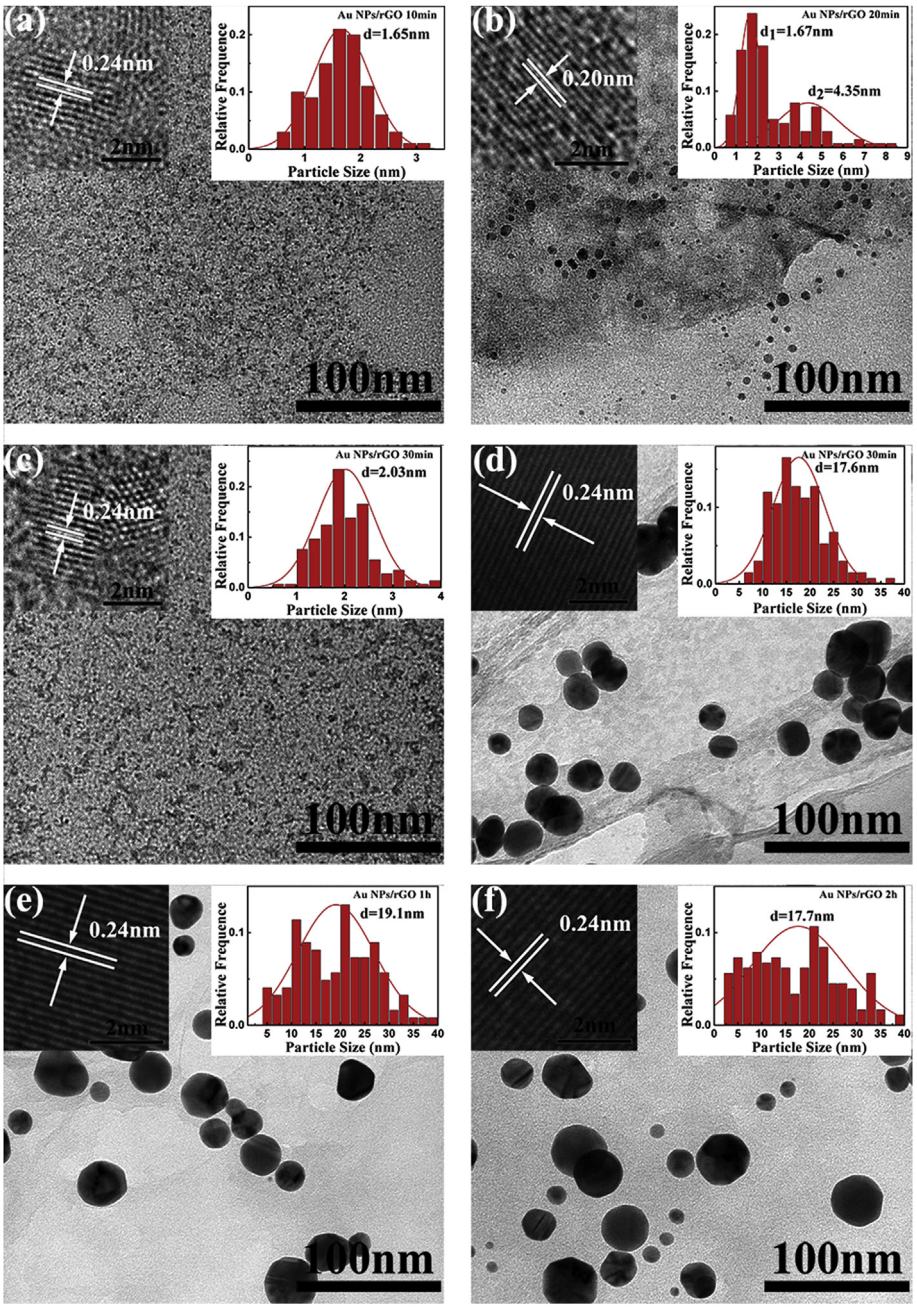

Fig. 2. TEM images of the AuNPs/rGO composites prepared with irradiation time of **(a)** 10 min, **(b)** 20min, **(c)** 30 min, **(d)** 30min, **(e)** 1 h, and **(f)** 2 h. The insets in the upper left corner show the corresponding HRTEM image of AuNPs. The insets in the upper right corner show the corresponding size distributions of the AuNPs. (A colour version of this figure can be viewed online.)

beam can be expressed as $\omega^2(z) = \omega_0{}^2\sqrt{1+z^2/z_0{}^2}$. While the input energy in different position is $I(z) = I/\pi\omega^2(z)$. In our experiment, the waist radius of the focus ω_0 was measured to be about 35 μm. By fitting the results of the Z-scan results (the line in Fig. 4(a) and (b)), we can obtain the values of I_s and β of samples, as shown in Table 1. For GO, rGO and AuNPs/rGO with an irradiation time of 30 min, the AuNPs/rGO has the lowest I_s value, indicating the AuNPs/rGO has an enhanced SA property compared with GO and rGO. Besides, with increasing the irradiation time, the values of I_s of AuNPs/rGO composites is decreased, indicating a more excellent SA property. The value of I_s in the AuNPs/rGO composites prepared using 2 h laser ablation was decreased by 1 order than that of rGO, and a large RSA coefficient as large as 5691 cm GW^{-1}. These results are comparable to those in previous reports [10]. It should be noted that, the I_s value for AuNPs/rGO 10 min is slightly increased (~2%) compared with GO. As the irradiation time is very short and the materials change very little, the slight change of I_s value could be attributed to the experimental errors.

Here, femtosecond laser pump-probe measurement was performed to investigate the mechanism of the enhancement of NLO properties and the photoinduced carriers dynamics between metal NPs and graphene, and the results of the AuNPs/rGO 30 min in a 1 mm thick quartz cuvette are given in Fig. 5(a). The pump and probe laser was centered at 800 nm and the pump pulse energy intensity was estimated to be about 3.2 mJ cm^{-2}. By fitting the results (the line in Fig. 5(a)), two distinct processes are observed: a

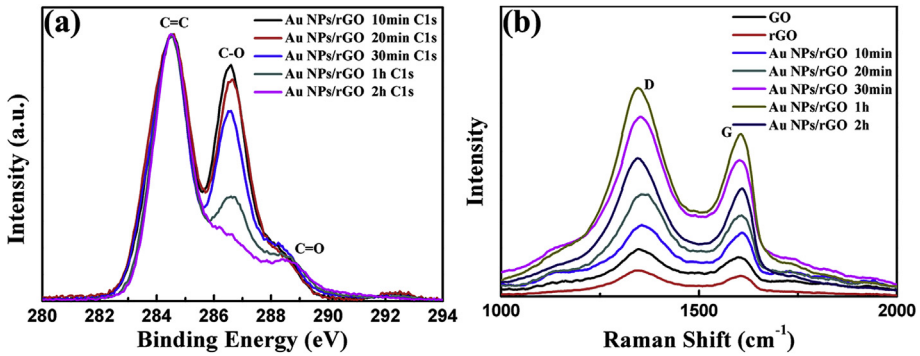

Fig. 3. **(a)** XPS spectra of C 1s of AuNPs/rGO prepared with different irradiation time. **(b)** Raman spectra of GO, rGO, and AuNPs/rGO composits with different irradiation time. (A colour version of this figure can be viewed online.)

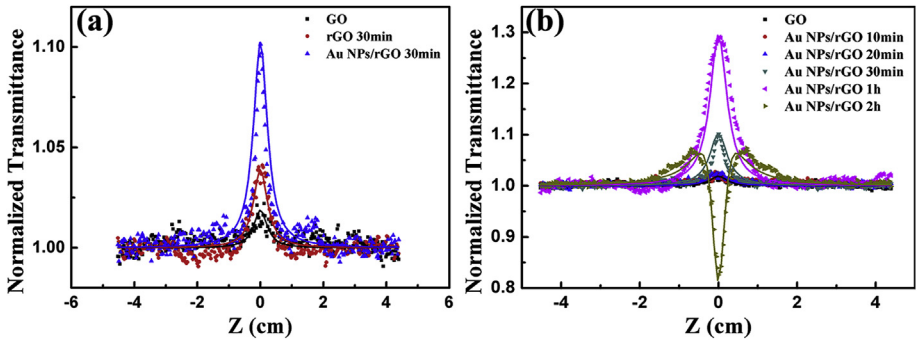

Fig. 4. **(a)** Z-scan results of GO, rGO, and AuNPs/rGO ablated for 30 min. **(b)** Z-scan results of AuNPs/rGO prepared with different irradiation time. (A colour version of this figure can be viewed online.)

Table 1
The comparison of I_s and β of GO, rGO, and AuNPs/rGO with different irradiation time.

Sample	I_s (GW cm^{-2})	β (cm GW^{-1})
GO	173.26	
rGO 30min	87.92	
AuNPs/rGO 10min	180.97	
AuNPs/rGO 20min	147.12	
AuNPs/rGO 30min	60.31	
AuNPs/rGO 1h	52.2	
AuNPs/rGO 2h	8.56	5691.19

dramatically fast decay process with a lifetimes of 1 ps and a slow relaxation process with a lifetime of 50 ps? In pure graphene, electrons in VB are easily excited to CB after intense light irradiation, causing the bleaching of VB and filling of CB. As a result, further absorption of the incident light is blocked leading to the SA effect [5,10]. In the previous report, the relaxation of nonequilibrium photogenerated carriers has been associated with two distinct processes: carrier-carrier scattering (70–120 fs) and carrier-phonon scattering (0.4–1.7 ps range) [34]. The fast decay process (~1 ps) observed in our experiments accordes well with the carrier-phonon scattering time scale in rGO, but the slow processes need further discussion.

When rGO is decorated with AuNPs, electron transfer takes place from AuNPs to graphene to achieve a common Fermi level [35]. Fig. 5(b) shows the energy band structure of the nanocomposites schematically. When graphene is excited by a pump laser (process (1)), the excited carriers in the CB of graphene will transfer to the sp band of AuNPs (process (2)) due to the considerably larger density of states in the AuNPs. Then these transferred carriers will return to the VB of graphene (process (3)) slowly. As has been demonstrated in previous report, the decay of the nonequilibrium distribution of photoexcited carriers in graphene through carrier-photon scattering ranges from 0.4 to 1.7 ps [34]. Hence the fast relaxation with 1 ps day time can be attributed to the lifetime of the excited carriers in the CB of graphene, while the slow relaxation with 50 ps is in accord with the decay time of the disctribution of the sp band of AuNPs [10,11,13].

Because the excited carriers in the CB of graphene will transfer to the sp band of AuNPs before return to the VB of graphene (processes (2, 3)), leading to a much longer carriers lifetime, the bleaching effect of graphene will be enhanced, resulting in an enhanced SA effect compared with pure graphene. When the femtosecond laser was used to fabricate the AuNPs/rGO hybrids, more AuNPs could be generated with increasing the irradiation time (as shown in Fig. 2). As a results, more metal states would be generated and the SA property would be increased. When the irradiation time is increased to 2 h, the size of AuNPs is relatively large. This will induce a strong two-photon absorption (2 PA) of AuNPs, causing the RSA effect in the hybrids [10,36,37]. The decay process of the RSA signal in AuNPs/rGO 30 min is also studied using pump-probe measurement under a pump laser energy of 19.2 mJ cm^{-2}. As shown in Fig. S6, the lifetime of the RSA process is estimated to be about 4 ps, which is consistent with the electron-phonon interaction time of pure AuNPs, proving the contribution of the 2 PA in AuNPs to the RSA effect in the composites [38].

Fs-TA measurement was further performed to verify the energy band model. Fig. 6 (a) shows the TA spectrum of AuNPs/rGO 30 min in a 1 mm thick quartz cuvette at a delay time of 3 ps with a pump power of 2 mW. Two negative absorption peaks centered at 525 nm and 647 nm and two positive absorption peaks centered at 485 nm

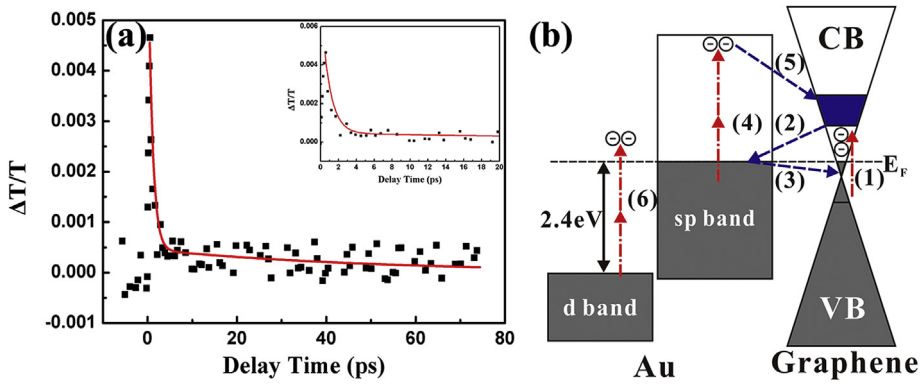

Fig. 5. **(a)** Femtosecond laser pump-probe result. **(b)** Energy band schematic diagram of AuNPs/rGO. The insets indicate the enlaraged curve. (A colour version of this figure can be viewed online.)

and near 740 nm can be observed. The positive spectra peaked at about 485 nm and negative absorption dip at about 525 nm can be attributed to the transient absorption of the AuNPs. The positive absorption centered at 485 nm is due to a strong "reduction" in the optical refection, which is commonly observed in noble metals [13]. The negative absorption peak of 525 nm is related to the SPR absorption in AuNPs due to the plasmonic oscillations in sp band. When intense laser irradiates to AuNPs/rGO, carriers in sp band are able to be excited to higher level (process (4)), causing the bleaching of low level and filling of high level, resulting in the reduction of absorption at around 525 nm. The time-resolved TA spectra are given in Fig. S7. As shown by the figure, the characteristic absorption peaks/valleys exhibit different temporal behavior. Fig. 6(b) indicates the TA dynamics measured at 525 nm probe wavelength, the decay process of which can be well fitted by a double-exponential function. The fast carriers transition process (~2 ps) is corresponding to the electron-phonon scattering in AuNPs/rGO, while the slow process (~670 ps) is corresponding to the interaction between AuNPs/rGO and surrounding solvent [11,12,39]. This result is consistent with previous reports [13].

Besides the typical TA peak and vallay at 485 and 525 nm in AuNPs [13], a negative dip at 647 nm and a positive peak at 740 nm are also observed in the TA spectra. Fig. 6 (c) and (d) show the TA dynamics of the hybrids at 647 nm and 740 nm, respectively. By fitting the results (the line in Fig. 6(c) and (d)), we can obtain the lifetimes of the two peaks, respectively. For 647 nm, two lifetimes of 8 ps and 1.1 ns are observed. We speculate that the featured TA spectra at 647 nm are attributed to the interaction between AuNPs and graphene. First, when pump laser irradiates to AuNPs/rGO, carriers below the Fermi level of graphene are excited to CB (process (1)), resulting in the bleaching VB and filling of CB. At the same time, carriers in the sp band of AuNPs can be excited to higher level (process (4)) by intraband excitation, then these excieted carriers transfer from AuNPs to the CB of graphene (process (5)). As a result, more carriers will fill in the CB of graphene as shown by the blue area in Fig. 5(b). When the probe laser incidents into the sample,

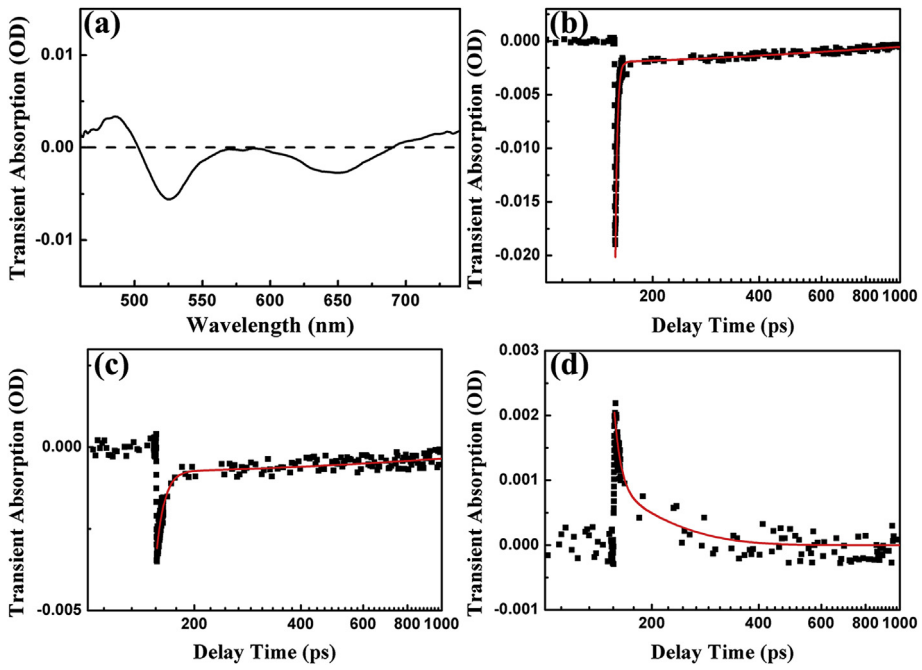

Fig. 6. **(a)** The TA of AuNPs/rGO as a function of probe wavelength with a pump power of 2 mW and a probe delay time of 3 ps? The TA of AuNPs/rGO as a function of probe delay time at wavelength of **(b)** 525 nm, **(c)** 647 nm and **(d)** 740 nm with a pump power of 2 mW. The insets indicate the enlaraged curve. (A colour version of this figure can be viewed online.)

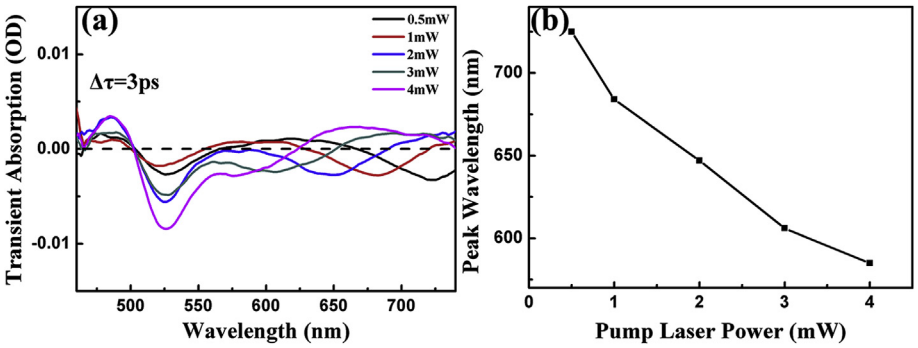

Fig. 7. **(a)** The TA of AuNPs/rGO as a function of probe wavelength with the pump laser power varying from 0.5 mW to 4 mW and a probe delay time of 3 ps? **(b)** The negative absorption peaks vary with the pump laser power. (A colour version of this figure can be viewed online.)

because the CB of the graphene has been further filled, the absorption of probe laser with higher energy will be reduced, resulting in a negative absorption. The decay process of 8 ps at 647 nm is mainly determined by the nonequilibrium carriers from the sp band of AuNPs. The slow decay process of 1.1 ns could be attributed to the interaction between AuNPs/rGO and surrounding solvent. The induced absorption above 740 nm can be due to a transient localized surface plasmon resonance (LSPR)-like absorption of excited carriers in the sp band of AuNPs [13]. To be different with the intrinsic plasmon, this pasmon resonance is induced by the interband excitation from d band to sp band of Au by 2 PA of 800 nm pump light. Two lifetimes are 7 ps and 80 ps are obtained by fitting the TA curve as shown in Fig. 6(d). The fast decay process is much longer than that of the intrinsic plasmon-bleaching dynamic at 525 nm (~2 ps). The prolonged decay process could mainly be due to the electron-phonon interaction of the interband-excitation induced holes in the d band and the hot electrons with the lattices [13].

The size of the AuNPs can also influence the carrier dynamics of the composites. The TA dynamics at 525 nm of AuNPs/rGO prepared with different irradiation time are given in Fig. S8, and the corresponding fitted lifetime is shown in Table S1. With increasing the irradiation, the size of AuNPs is increased, and the liftetime of the photoinduced bleaching signals at 525 nm is reduced. Because of the large density of states in larger AuNPs, the excited electrons are more easily recombined with holes in sp band, and the decay process of the bleaching signal becomes fast. Benefiting from the large states density in the AuNPs, the excited carriers in the CB of graphene are more likely to transfer to the AuNPs through process (2) shown in Fig. 5(b), causing the enhancement of the SA effect.

To further verify our predictions, TA spectra as a function of the pump power are measured. As shown in Fig. 7(a), a clear peak shift from 725 nm to 585 nm can be observed with the pump laser power varying from 0.5 mW to 4 mW. Fig. 7(b) shows the curve of negative absorption peak varies with the pump laser power. With increasing the pump laser power, the excited carriers in sp band of AuNPs (process (4)) will be increased. Then, more carriers will transfer from AuNPs to the CB of graphene (process (5)) and the highest energy level in CB will be raised, as the blue area shown in Fig. 5(b). As a result, the absorption edge of the excited graphene is blue shifted. This results are corresponding to the proposed energy band model.

4. Conclusion

In summary, the AuNPs/rGO nanocomposites was successfully synthesized using LAL method by ablating the mixed aqueous solutions of $HAuCl_4$ and GO using femtosecond laser pulses. The significant enhancement of NLO response of nanocomposites was demonstrated using Z-scan method by femtosecond laser. The carriers dynamics was clarified using a femtosecond laser pump-probe technique and a TA measurements, respictively. The results show that the enhancement of NLO properties of graphene is due to a long lifetime process which is attributed to the intersystem transition from the CB of graphene to the sp band of AuNPs. Besides, a shifted negative absorption peak varying with the pump laser power which is due to intersystem transition from the sp band of AuNPs to the CB of graphene was observed.

Acknowledgements

This work was supported by National R&D Program of China (2017YFA0207400), and National Natural Science Foundation of China (61690221, 61427816, 11674260), and the Fundamental Research Funds for the Central Universities, and the Collaborative Innovation Center of Suzhou Nano Science and Technology. The TEM work was performed at the International Center for Dielectric Research (ICDR), Xi'an Jiaotong University, Xi'an, China. The authors also thank Mr. Ma and Ms. Lu for their help in using TEM.

Appendix A. Supplementary data

Supplementary data to this article can be found online at https://doi.org/10.1016/j.carbon.2019.03.054.

References

[1] X. Jiang, L. Polavarapu, S.T. Neo, T. Venkatesan, Q. Xu, Graphene oxides as tunable broadband nonlinear optical materials for femtosecond laser pulses, J. Phys. Chem. Lett. 3 (6) (2012) 785–790.
[2] R. Raccichini, A. Varzi, S. Passerini, B. Scrosati, The role of graphene for electrochemical energy storage, Nat. Mater. 14 (3) (2015) 271–279.
[3] F. Bonaccorso, L. Colombo, G. Yu, M. Stoller, V. Tozzini, A.C. Ferrari, et al., Graphene, related two-dimensional crystals, and hybrid systems for energy conversion and storage, Science 347 (6217) (2015) 1246501.
[4] A.H. Castro Neto, F. Guinea, N.M.R. Peres, K.S. Novoselov, A.K. Geim, The electronic properties of graphene, Rev. Mod. Phys. 81 (1) (2009) 109–162.
[5] Q. Bao, H. Zhang, Y. Wang, Z. Ni, Y. Yan, Z.X. Shen, et al., Atomic-layer graphene as a saturable absorber for ultrafast pulsed lasers, Adv. Funct. Mater. 19 (19) (2009) 3077–3083.
[6] A. Martinez, Z. Sun, Nanotube and graphene saturable absorbers for fibre lasers, Nat. Photon. 7 (11) (2013 2013-01-01) 842–845.
[7] V. Georgakilas, J.N. Tiwari, K.C. Kemp, J.A. Perman, A.B. Bourlinos, K.S. Kim, et al., Noncovalent functionalization of graphene and graphene oxide for energy materials, biosensing, catalytic, and biomedical applications, Chem. Rev. 116 (9) (2016) 5464–5519.
[8] D. Gu, X. Chang, X. Zhai, S. Sun, Z. Li, T. Liu, et al., Efficient synthesis of silver-reduced graphene oxide composites with prolonged antibacterial effects, Ceram. Int. 42 (8) (2016) 9769–9778.
[9] S. Fraser, X. Zheng, L. Qiu, D. Li, B. Jia, Enhanced optical nonlinearities of hybrid graphene oxide films functionalized with gold nanoparticles, Appl. Phys. Lett. 107 (3) (2015) 31112.

[10] B.S. Kalanoor, P.B. Bisht, S. Akbar Ali, T.T. Baby, S. Ramaprabhu, Optical nonlinearity of silver-decorated graphene, J. Opt. Soc. Am. B 29 (4) (2012) 669.
[11] S. Kumar, M. Anija, N. Kamaraju, K.S. Vasu, K.S. Subrahmanyam, A.K. Sood, et al., Femtosecond carrier dynamics and saturable absorption in graphene suspensions, Appl. Phys. Lett. 95 (19) (2009) 191911.
[12] D. Giovanni, G. Yu, G. Xing, M.L. Leek, T.C. Sum, Measurement of sub-10 fs Auger processes in monolayer graphene, Optic Express 23 (16) (2015) 21107.
[13] X. Zhang, C. Huang, M. Wang, P. Huang, X. He, Z. Wei, Transient localized surface plasmon induced by femtosecond interband excitation in gold nanoparticles, Sci. Rep. 8 (1) (2018) 10499.
[14] D. Zhang, B. Gökce, Perspective of laser-prototyping nanoparticle-polymer composites, Appl. Surf. Sci. 392 (2017) 991–1003.
[15] V. Nguyen, L. Yan, H. Xu, M. Yue, One-step synthesis of multi-emission carbon nanodots for ratiometric temperature sensing, Appl. Surf. Sci. 427 (2018) 1118–1123.
[16] D. Zhang, J. Liu, P. Li, Z. Tian, C. Liang, Recent advances in surfactant-free, surface-charged, and defect-rich catalysts developed by laser ablation and processing in liquids, ChemNanoMat 3 (8) (2017) 512–533.
[17] A.R. Sadrolhosseini, A.S.M. Noor, N. Faraji, A. Kharazmi, M.A. Mahdi, Optical nonlinear refractive index of laser-ablated gold nanoparticles graphene oxide composite, J. Nanomater. 2014 (2014) 1–8.
[18] V. Nguyen, L. Yan, J. Si, X. Hou, Femtosecond laser-induced size reduction of carbon nanodots in solution: effect of laser fluence, spot size, and irradiation time, J. Appl. Phys. 117 (8) (2015) 84304.
[19] J.I. Paredes, S. Villar-Rodil, A. Martínez-Alonso, J.M.D. Tascón, Graphene oxide dispersions in organic solvents, Langmuir 24 (19) (2008 2008-10-07) 10560–10564.
[20] Y. Yang, J. Shi, G. Kawamura, M. Nogami, Preparation of Au-Ag, Ag-Au core-shell bimetallic nanoparticles for surface-enhanced Raman scattering, Scripta Mater. 58 (10) (2008) 862–865.
[21] J. Park, M. Atobe, T. Fuchigami, Sonochemical synthesis of conducting polymer-metal nanoparticles nanocomposite, Electrochim. Acta 51 (5) (2005) 849–854.
[22] H. Jie, Z. Liming, C. Biao, J. Nan, C. Fenghua, Z. Yi, et al., Nanocomposites of size-controlled gold nanoparticles and graphene oxide: formation and applications in SERS and catalysis, Nanoscale 2 (12) (2010) 2733–2738.
[23] M.M. Giangregorio, M. Losurdo, G.V. Bianco, E. Dilonardo, P. Capezzuto, G. Bruno, Synthesis and characterization of plasmon resonant gold nanoparticles and graphene for photovoltaics, Mater. Sci. Eng. B-Adv. 178 (9SI) (2013) 559–567.
[24] S.L. Logunov, T.S. Ahmadi, M.A. ElSayed, J.T. Khoury, R.L. Whetten, Electron dynamics of passivated gold nanocrystals probed by subpicosecond transient absorption spectroscopy, J. Phys. Chem. B 101 (19) (1997) 3713–3719.
[25] L. Yang, N. Huang, Q. Lu, M. Liu, H. Li, Y. Zhang, et al., A quadruplet electrochemical platform for ultrasensitive and simultaneous detection of ascorbic acid, dopamine, uric acid and acetaminophen based on a ferrocene derivative functional Au NPs/carbon dots nanocomposite and graphene, Anal. Chim. Acta 903 (2016) 69–80.
[26] X. Lu, L. Tao, D. Song, Y. Li, F. Gao, Bimetallic Pd@Au nanorods based ultrasensitive acetylcholinesterase biosensor for determination of organophosphate pesticides, Sensor. Actuator. B Chem. 255 (2018) 2575–2581.
[27] S. Moussa, G. Atkinson, M. SamyEl-Shall, A. Shehata, K.M. AbouZeid, M.B. Mohamed, Laser assisted photocatalytic reduction of metal ions by graphene oxide, J. Mater. Chem. 21 (26) (2011) 9608.
[28] V. Abdelsayed, S. Moussa, H.M. Hassan, H.S. Aluri, M.M. Collinson, M.S. El-Shall, Photothermal deoxygenation of graphite oxide with laser excitation in solution and graphene-aided increase in water temperature, J. Phys. Chem. Lett. 1 (19) (2010) 2804–2809.
[29] A.Y. Klyushin, T.C.R. Rocha, M. Hävecker, A. Knop-Gericke, R. Schlögl, Near ambient pressure XPS study of Au oxidation, Phys. Chem. Chem. Phys. 16 (17) (2014) 7881.
[30] X. Liu, L. Cao, W. Song, K. Ai, L. Lu, Functionalizing metal nanostructured film with graphene oxide for ultrasensitive detection of aromatic molecules by surface-enhanced Raman spectroscopy, Acs. Appl. Mater. Inter. 3 (8) (2011) 2944–2952.
[31] J. Huang, C. Zong, H. Shen, M. Liu, B. Chen, B. Ren, et al., Mechanism of cellular uptake of graphene oxide studied by surface-enhanced Raman spectroscopy, Small 8 (16) (2012) 2577–2584.
[32] H. Zhang, S.B. Lu, J. Zheng, J. Du, S.C. Wen, D.Y. Tang, et al., Molybdenum disulfide (MoS2) as a broadband saturable absorber for ultra-fast photonics, Optic Express 22 (6) (2014) 7249.
[33] B. Qu, Q. Ouyang, X. Yu, W. Luo, L. Qi, Y. Chen, Nonlinear absorption, nonlinear scattering, and optical limiting properties of MoS2-ZnO composite-based organic glasses, Phys. Chem. Chem. Phys. 17 (8) (2015) 6036–6043.
[34] J.M. Dawlaty, S. Shivaraman, M. Chandrashekhar, F. Rana, M.G. Spencer, Measurement of ultrafast carrier dynamics in epitaxial graphene, Appl. Phys. Lett. 8 (4) (2008) 42116, 92.
[35] K.S. Subrahmanyam, A.K. Manna, S.K. Pati, C.N.R. Rao, A study of graphene decorated with metal nanoparticles, Chem. Phys. Lett. 497 (1–3) (2010) 70–75.
[36] R. Philip, P. Chantharasupawong, H. Qian, R. Jin, J. Thomas, Evolution of nonlinear optical properties: from gold atomic clusters to plasmonic nanocrystals, Nano Lett. 12 (9) (2012) 4661–4667.
[37] R. Ho-Wu, S.H. Yau, T. Goodson, Linear and nonlinear optical properties of monolayer-protected gold nanocluster films, ACS Nano 10 (1) (2015) 562–572.
[38] H.J. Shin, I. Hwang, Y. Hwang, D. Kim, S.H. Han, J. Lee, et al., Comparative investigation of energy relaxation dynamics of gold nanoparticles and gold-polypyrrole encapsulated nanoparticles, J. Phys. Chem. B 107 (20) (2003) 4699–4704.
[39] T.W. Roberti, B.A. Smith, J.Z. Zhang, Ultrafast electron dynamics at the liquid-metal interface: femtosecond studies using surface plasmons in aqueous silver colloid, J. Chem. Phys. 102 (9) (1995) 3860–3866.